



# Suspended sediment budget and intra-event sediment dynamics of a small glaciated mountainous catchment in the Northern Caucasus

Anatoly Tsyplenkov<sup>1,2</sup> · Matthias Vanmaercke<sup>3</sup> · Valentin Golosov<sup>1,2,4</sup> · Sergey Chalov<sup>1</sup>

Received: 13 January 2020 / Accepted: 19 April 2020  
© Springer-Verlag GmbH Germany, part of Springer Nature 2020

## Abstract

**Purpose** The sediment dynamics of (peri-)glacial catchments can be highly variable and complex. Understanding these dynamics and their underlying causes is not only of interest from a scientific perspective but also required to address the practical problems with which they are often associated. In order to better understand the sediment dynamics of glaciated mountainous catchments, suspended sediment fluxes in the 9.1 km<sup>2</sup> Djankuat catchment (North Caucasus, Russia) were monitored intensively during the 2017 ablation season.

**Materials and methods** The intra-event suspended sediment dynamics were studied using a newly proposed simple hysteresis index (*SHI*), quantifying to what extent evolutions in sediment concentration are characterized by a clockwise or anticlockwise hysteresis loop.

**Results and discussion** The resulting catchment suspended sediment yield was 1033 t km<sup>-2</sup> year<sup>-1</sup>, with the glacier itself contributing 72% of the suspended sediment load. However, during rainfall events, also hillslope erosion in the proglacial area became a very significant sediment source. Clockwise hysteresis loops occurred in 61.8% of the events, while anticlockwise in 11.8%. On the other hand, only 47.8% of the total suspended sediment flux was transported during clockwise events. Our observations clearly indicate that events showing a stronger clockwise pattern (i.e., a higher *SHI*) are associated with a larger sediment input from the proglacial area.

**Conclusions** Overall, our results provide data and insights on sediment dynamics in an understudied environment. They illustrate that the type and characteristics of sediment concentration hysteresis loops are to some extent linked to the dominant sediment sources during the event. As such, the proposed methodology and *SHI* may also help with a better understanding of sediment dynamics in other environments.

---

Responsible editor: Hugh Smith

---

**Electronic supplementary material** The online version of this article (<https://doi.org/10.1007/s11368-020-02633-z>) contains supplementary material, which is available to authorized users.

---

✉ Anatoly Tsyplenkov  
atsyplenkov@gmail.com

<sup>1</sup> Faculty of Geography, Lomonosov Moscow State University, Leninskiye Gory, 1, Moscow, Russian Federation 119991

<sup>2</sup> Institute of Geography, Russian Academy of Sciences, Staromonetny st. 29, Moscow, Russian Federation 119017

<sup>3</sup> Département de Géographie, Université de Liège, U.R. SPHERES, Clos Mercator 3, 4000 Liège, Belgium

<sup>4</sup> Kazan Federal University, Kremlevskaya st., 18, Kazan, Russian Federation 420008

**Keywords** Sediment yield · Hysteresis · Mountain hydrology · Suspended sediments · Sediment budget

## 1 Introduction

Over the past decades, there has been an increasing interest in the response of fluvial sediment system to climate change (e.g., Walling 1995; Jones 1999; Farnsworth and Milliman 2003; Koppes and Montgomery 2009; Glazirin and Semakova 2019). One of the key elements in this response are glaciers and their influence on the catchment sediment yield (*SY*) of mountainous headwaters (Beniston 2003; Barry 2006). Glaciers are generally a much more efficient erosion agent than rivers (e.g., Koppes and Montgomery 2009). They are, therefore, a dominant sediment source in many mountain

catchments (e.g., Gurnell et al. 1996; Hallet et al. 1996) and can exert a strong control on the *SY* of even larger river systems (e.g., Syvitski and Milliman 2007; Hinderer 2012).

While the *SY* values from glaciated catchments often rank amongst the highest in the world (e.g., Dedkov and Moszherin 1984; Hallet et al. 1996; Slaymaker 2018), it is also known that the sediment dynamics of (peri-)glacial catchments can be highly variable and complex (Warburton 1990; Gurnell et al. 1996; Hodgkins et al. 2003; Singh et al. 2005; Mano et al. 2009; O'Farrell et al. 2009; Iida et al. 2012; Mao and Carrillo 2017). Understanding these dynamics and their underlying causes is not only of interest from a scientific perspective but also required to address the practical problems with which they are often associated. These include damage to hydroelectric power plants, lake and reservoir sedimentation, irrigation canal aggradation, and impacts on water quality (e.g. Bogen 1989; Moore et al. 2009).

This need for a better understanding of sediment dynamics from glaciated catchments becomes even more relevant in the light of climate change (e.g., Morche et al. 2019). Ongoing glacier retreat will likely increase suspended sediment concentration in many proglacial streams due to an increase in subglacial sources and the paraglacial conditions resulting from glacial retreat (Moore et al. 2009). As such, not only the glaciers itself but also the (typically barren) hillslopes and moraine deposits in the direct vicinity of the glacier can be an important sediment source (Carrivick et al. 2013; Geilhausen et al. 2013; Morche et al. 2019). Expected changes in precipitation regime and intensity (e.g., Stott and Mount 2007; Polade et al. 2015) can be expected to affect the significance of such sediment sources, leading to further complexity.

Nonetheless, only a limited number of case studies exist on the sediment budget of glaciated catchments (e.g., Warburton 1990; Otto et al. 2009; O'Farrell et al. 2009; Leggat et al. 2015; Mao and Carrillo 2017). This is especially the case for the Caucasus. Although a significant number of works have studied the denudation and river sediment yield in this mountain range (Khmeleva et al. 2000; Jaoshvili 2002; Khmeleva and Shevchenko 2006; Vinogradova et al. 2007; Mozzherin and Sharifullin 2015), only very few provide sediment budgets for glaciated basins (e.g., Durgerov et al. 1972). Nevertheless, also in the Caucasus, most glaciers retreat (Solomina 2000; Stokes et al. 2007; Kutuzov and Shahgedanova 2009; Tielidze et al. 2015; Kutuzov et al. 2019). This happens at an increasing rate: from  $-0.44\%$  year<sup>-1</sup> areal change in 1960–1986 to  $-0.69\%$  year<sup>-1</sup> in 1986–2014 (Tielidze and Wheate 2018). As discussed above, this can be expected to elevate the total sediment yield of the region in the future.

Moreover, very few studies have focused on sediment dynamics at the intra-event scale. Nonetheless, sediment discharge events are typically characterized by suspended sediment concentration (*SSC*, [ $\text{g m}^{-3}$ ])–runoff discharge (*Q*,

[ $\text{m}^3 \text{s}^{-1}$ ]) hysteresis loops. Such hysteresis loops can have a significant impact on the accuracy of total suspended sediment loads and should therefore be accounted for (e.g., Morehead et al. 2003; Vanmaercke et al. 2010). However, it is also expected that they can provide insight into the dominant sediment sources during the event (e.g., Morehead et al. 2003; Lloyd et al. 2016).

Also, in the case of glaciated catchments, hysteresis effects are frequently observed. Several researchers (e.g., Singh et al. 2005; Iida et al. 2012) suggest that clockwise hysteresis loops dominate during the entire ablation period. On the other hand, Mao and Carrillo (2017) report that, for the small Andean catchment they studied, clockwise hysteresis loops mainly occur during snowmelt events, while anticlockwise loops prevail during glacier melting. Furthermore, Favaro and Lamoureux (2015) indicate that hysteresis patterns can change because of global warming. Their study in the High Arctic (2004–2012) has shown that daily hysteresis patterns shifted from dominantly clockwise to a more frequent occurrence of anticlockwise loops. Nonetheless, it remains unclear to what extent these findings can be generalized, given the currently limited number of case studies available that systematically analyze the temporal dynamics of sediment concentrations across a sufficiently large number of events.

In addition, the study of hysteresis patterns in relation to sediment sources is often difficult because it is not always straightforward to characterize or quantify hysteresis loops. This is especially so when the number of observations during the event is limited (e.g., Vanmaercke et al. 2010). To mitigate this challenge, several studies have prepared hysteresis indexes (Langlois et al. 2005; Lawler et al. 2006; Lloyd et al. 2016). These indexes typically come with limitations. For example, they do not always clearly depend on the magnitude of the event (Langlois et al. 2005; Lawler et al. 2006), which restricts their capability to quantify the importance of different hysteresis types for sediment transport. Later studies have proposed improvements (Gao and Josefson 2012). However, such improvements also come with the requirement of more measurements (e.g., Lloyd et al. 2016; Hamshaw et al. 2018). Nonetheless, the dominant hysteresis pattern can usually be determined with a relatively limited number of samples (Aich et al. 2014).

To help address these research gaps, this paper investigates the suspended sediment dynamics of the Djankuat, a glaciated mountainous catchment located in the North Caucasus (Russia). Based on a large set of measurements, we aim to quantify the total suspended sediment load as well as the relative importance of different sediment sources at both the seasonal and event scales. For the latter, we propose a new method/index to quantify runoff discharge–sediment concentration hysteresis loops that can also be applied when only a small number of samples are available.

## 2 Study area

Our research was conducted at the Djankuat Glaciological Station (DGS), located at the Russian part of Northern Caucasus, near the Russian-Georgian border (43° 12' 31.71" N, 42° 44' 05.93" E, altitude 2635 m). The Djankuat catchment was selected as a representative case study for the Northern Caucasus during the International Hydrological Decade (Dyrgerov 2003). Detailed observations on the glaciology, meteorology, and hydrology of the catchment have been made since 1965. It is therefore one of the best-studied glaciers in Russia (Stokes et al. 2007; Lavrentiev et al. 2015; Vasil'chuk et al. 2016; Rets et al. 2017; Toropov et al. 2017; Rybak and Rybak 2018). Nonetheless, our understanding of its sediment dynamics has remained very limited. Continuous *SSC* measurements have only been conducted since 2015 (Rets et al. 2019).

The Djankuat catchment is a typical high mountain catchment with steep slopes, alpine meadows, and glacial-nival terrains. Its catchment area is 9.1 km<sup>2</sup>. In 2017, 27% of its surface area was covered by glaciers (Rets et al. 2019; Table 1). The largest glacier (2.42 km<sup>2</sup>), i.e., the Djankuat glacier, is the source of the Djankuat river (cf. Fig. 1). In addition, there are three smaller glaciers (<0.5 km<sup>2</sup>) located in the study basin: Koiavgan, Viatau, and Visyachii. The average precipitation depth (in rainfall equivalents) is around 4090 mm year<sup>-1</sup>. However, precipitation is characterized by an important temporal variability with daily amounts up to 97.2 mm day<sup>-1</sup>. During the ablation period (May–September) at the DGS air temperature ranges from -1.1 to 24.2 °C with an average of 10.2 °C. At the glacier (3000 m) temperature during this period ranges from -9 to 17.6 °C with an average of 6.6 °C (Rets et al. 2019).

Typically, the catchment is almost completely covered with snow until late May–early June, when the melting season begins. At the beginning of July, only a few patches of snow remain at the higher elevations and north-facing slopes of the non-glaciated area. Due to this specific hydrological regime, an estimated 98% of the total sediment flux and water runoff occurs in the ablation period (Dyrgerov et al. 1972; Rets et al. 2017).

Mean water discharge at the outlet of the Djankuat catchment is 1.38 m<sup>3</sup> s<sup>-1</sup>, with typical water discharges ranging

between 1 and 2 m<sup>3</sup> s<sup>-1</sup> (Rets et al. 2019). Peak discharges can reach values up to 3–4 m<sup>3</sup> s<sup>-1</sup>. Such high values are mostly observed in the second half of the ablation period and are often linked to high intensity rainfall events (Rets et al. 2019). Earlier work indicates that snow and ice-melting processes are, with 44%, the main sources of runoff in the catchment; 37% comes from groundwater and only 19% of the discharge is due to rainfall events (Rets et al. 2017).

## 3 Materials and methods

### 3.1 Layout of the stations and field data collection

All fieldwork was carried out during the ablation period of 2017. Runoff discharge ( $Q$ , m<sup>3</sup> s<sup>-1</sup>) and turbidity ( $T$ , NTU) were monitored at the downstream gauging station of the Djankuat (OUT, cf. Fig. 1) from June 6, 2017, to September 24, 2017. A digital pressure logger (Solinst Levellogger Junior) recorded the pressure (water and atmospheric) every 10 min. In addition, water stages ( $H$ , cm) were measured manually at 9:00, 11:00, 13:00, 15:00, 17:00, 19:00, 21:00, and 23:00 every day. These data allowed the conversion of the automatic pressure readings to flow depths and to verify the correct functioning of the pressure logger. Nearly 60 water discharge ( $Q$ ) measurements were made based on the dilution method, using NaCl as a tracer (Dobriyal et al. 2017). Based on these measurements, a robust stage-discharge ( $H$ - $Q$ ) relationship was developed, which allowed the conversion of observed flow depths into runoff discharges (for details; see Rets et al. 2019). To account for potential changes in bed morphology,  $H$ - $Q$  rating curves were established for every month of the measuring period (Rets et al. 2019).

Turbidity measurements were made at least eight times per day at the same times of the manual  $H$  recordings, using a portable turbidimeter Hach 2100P. To convert optical turbidity values ( $T$ , NTU) to suspended sediment concentration (*SSC*, g m<sup>-3</sup>), we established an empirical relationship between both variables. During the fieldwork campaigns in the ablation seasons of 2015–2017, we collected 39 water samples at the same time and location as the  $T$  measurements. These samples were filtered with a Millipore vacuum pump, using 0.45 μm Millipore membrane filter papers. These papers were then dried for 2 h at 105 °C and weighted. Based on this weight and the volume of the water sample, the *SSC* could be derived and compared with the corresponding  $T$ . Based on this comparison, the following empirical relationships were established (Fig. 2):

$$SSC = \begin{cases} 19 - 0.217 \cdot T + 0.00226 \cdot T^2, & T < 1000 \\ -556 + 1.21 \cdot T, & T \geq 1000 \end{cases} \quad (1)$$

**Table 1** Some key characteristics of the stream draining to the three gauging stations (cf. Fig. 1)

	OUT	MID	GL
Area (km <sup>2</sup> )	9.1	8.09	4.24
Minimum elevation (m)	2648	2682	2722
Maximum elevation (m)	3848	3848	3848
Elevation range (m)	1200	1166	1115
Glacierized area (%)	27	30.4	58.0

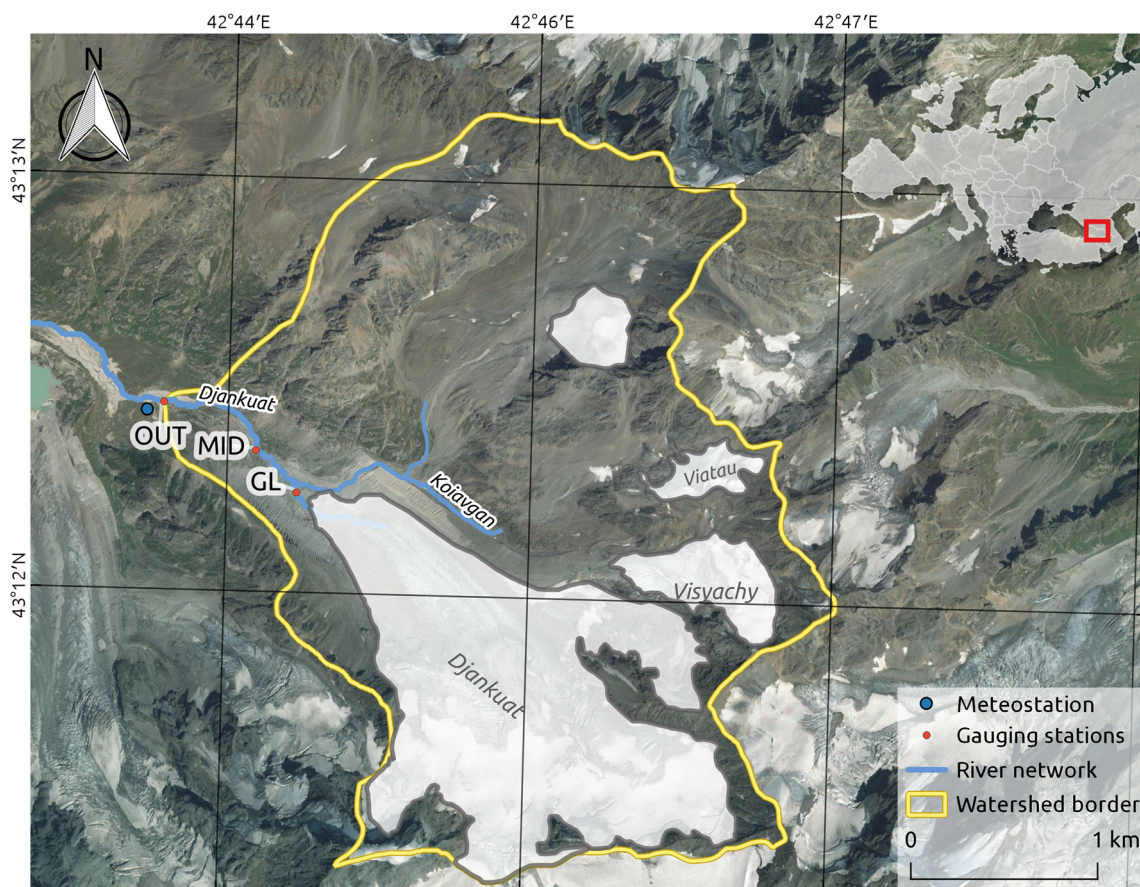


**Fig. 1** Overview of the Djankuat catchment and position of the gauging stations and meteorological stations used in this study. OUT gauging station at the catchment outlet, GL gauging station at the glacier mouth,

MID gauging station between OUT and GL (Source Satellite image: Worldview 2, 2010-08-20)

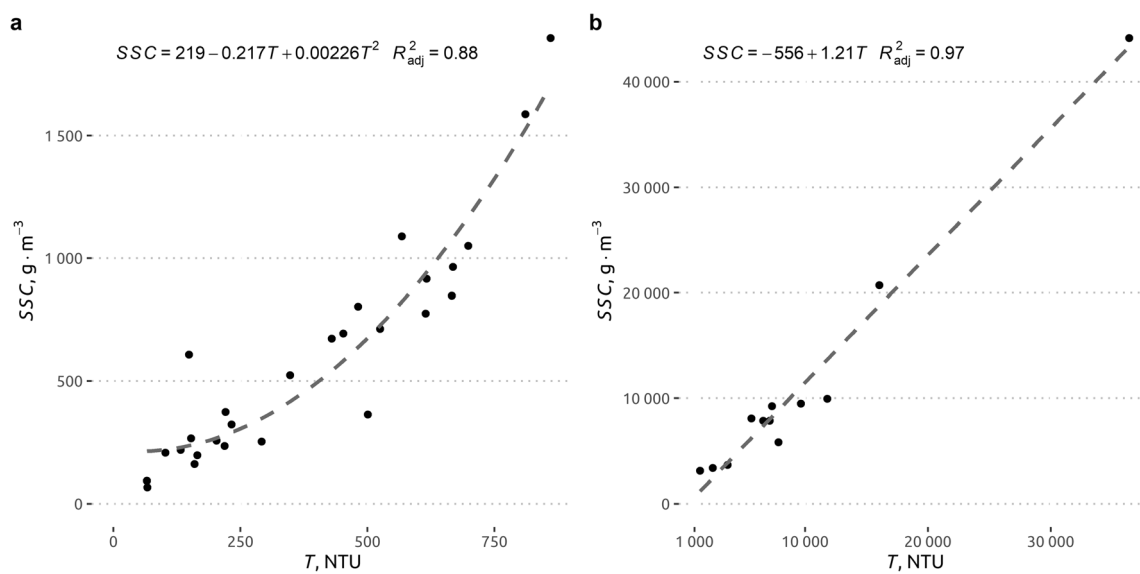


**Fig. 2** Suspended sediment concentration (SSC)–turbidity (T) relationships, based on 39 water samples collected between 2015 and 2017. A distinction is made for samples corresponding with a  $T < 1000$  NTU (a) and samples with a  $T$  above 1000 NTU (b)

where  $SSC$  is the suspended sediment concentration ( $\text{g m}^{-3}$ ) and  $T$  is the optical turbidity (NTU).

At the MID and GL stations (cf. Fig. 1), measurements were conducted from June 30, 2017, to August 30, 2017. At the MID station, only the water turbidity ( $T_{MID}$ , NTU) was measured. At the GL station, both turbidity ( $T_{GL}$ , NTU) and water stage ( $H_{GL}$ , cm) were measured. The  $T$ -observations at the GL and MID station were converted to  $SSC$  values, using Eq. 1 (Fig. 2). Typically, these measurements were conducted only twice a day (morning and evening). In general, they were conducted at the same time (within a 5–10-min interval) of each other and the measurements conducted at the OUT station.

Meteorological data for the measuring period are available in the database compiled by Rets et al. (2019). In this research, we used daily precipitation depths (in water equivalents), which were manually measured for every precipitation event near the outlet (Fig. 1). The rain gauge was located 0.5 m above ground.

Overall, suspended sediments at the outlet of the Djankuat catchment (OUT) can originate from four potential sources: the main glacier, the smaller glaciers (drained by the Koiavgan stream; Fig. 1), riverbed erosion and hillslope erosion (during snowmelt and rainfall events). Given its position, the only potential sediment source at the GL station is the main glacier. For the MID station, the potential sediment sources are similar as for the OUT station. However, given that measurements at MID (and GL) only started in the middle of the ablation season (July), the role of snowmelt as a potential runoff and sediment source was already negligible (Vasil'chuk et al. 2016).

### 3.2 Runoff discharge estimations for the GL and MID stations

While discharge was monitored continuously at the outlet of the catchment (OUT), continuous runoff discharge series were lacking for the GL and MID stations (cf. Fig. 1) and had to be estimated. For the GL station, we based our estimate on the assumption that, during days without rain, the dominant sediment sources at the OUT station is typically the main glacier (i.e., Djankuat glacier). This is justified by the fact that snowmelt was no longer significant when the measurements at the GL and MID station started (see above) and the relatively much smaller size of the small glaciers drained by the Koiavgan stream (cf. Study area; Fig. 1). In addition, visual inspections (and irregular  $T$  measurements) clearly indicated that water coming from the Koiavgan stream typically contained no significant amounts of sediments ( $\approx 10$ – $20$  NTU) during non-rainy days. We further hypothesized that, during non-rainy days, there is no significant deposition of suspended sediments between the GL and OUT station. This is justified by the short distance ( $\approx 1$  km) between both stations, the steep channel slope ( $\approx 100$  m  $\text{km}^{-1}$ ), the high observed stream velocities ( $1$ – $2$  m  $\text{s}^{-1}$ ), and the overall fine texture of the sediments (clay to silt). From these assumptions, it follows that the sediment discharge at the OUT stations during

non-rainy days ( $Q_{OUT} \times SSC_{OUT}$ ) should be about equal to the sediment discharge of the GL station ( $Q_{GL} \times SSC_{GL}$ ). As a consequence, the ratio  $SSC_{OUT}/SSC_{GL}$  should be equal to  $Q_{OUT}/Q_{GL}$ . As such, this allowed for the estimation  $Q_{GL}$ , based on observed  $Q_{OUT}$ ,  $SSC_{OUT}$ , and  $SSC_{GL}$  values during non-rainy days.

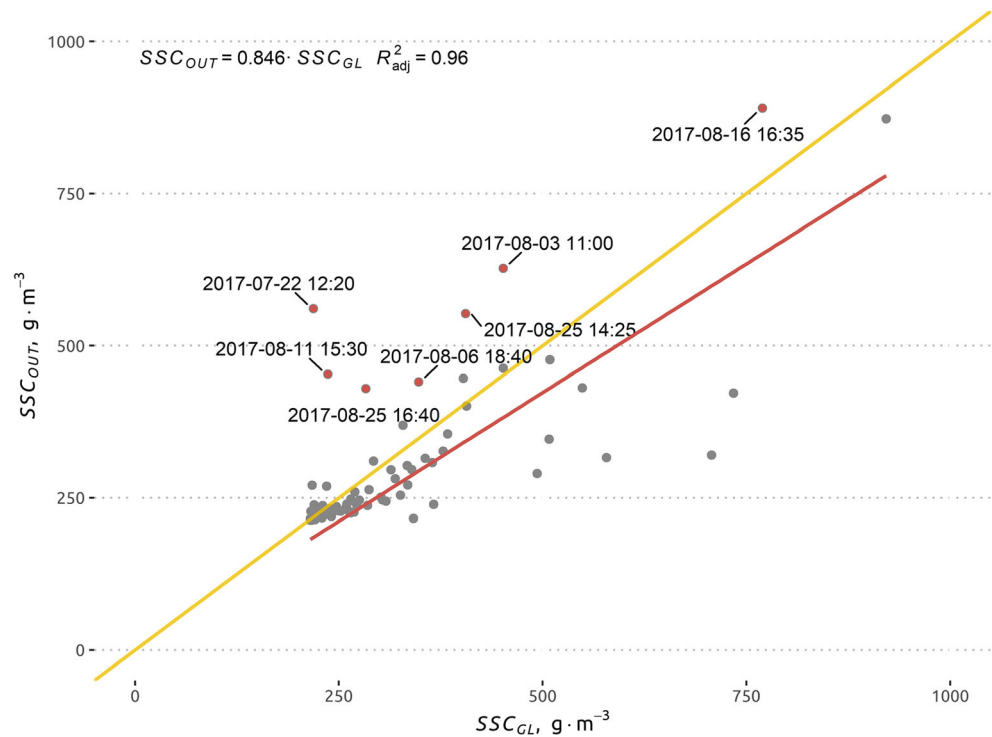
We therefore isolated all measurements conducted during days without rainfall (considering also the average concentration time of runoff) and compared the concentrations measured at the outlet ( $SSC_{OUT}$ ) with those measured at the glacier mouth ( $SSC_{GL}$ ). The resulting scatterplot (Fig. 3) reveals some outliers with clearly higher  $SSC$  concentrations at the OUT station. These are likely linked to mass wasting events in the Koiavgan tributary and/or channel erosion in the river section between the MID and OUT station. Nonetheless, as expected, concentrations at the OUT stations are typically lower than at the GL station. A simple linear relationship excluding these outliers indicates that sediment concentrations at the OUT station are on average 15% lower than those at the GL station. Following the reasoning above, this would imply that, on non-rainy days, 85% of the runoff discharge at the OUT station originates from the glacier mouth (GL) (i.e., melt water). Generic hydrograph separation of the Djankuat river at the end of the ablation season in 2014 showed similar values (70–80%; Rets et al. 2017). From this we calculated  $Q_{GL}$  as  $0.85 \times Q_{OUT}$  during non-rainy days. These estimated discharges at the glacier outlet could be confronted with their corresponding observed flow depth ( $H_{GL}$ ) to establish a depth-discharge rating curve for the GL station (Fig. 4b). While the adjusted  $R^2$  value of this rating curve is rather low ( $R^2_{adj} = 0.58$ ), it is still acceptable and comparable to the  $R^2$  values for the H–Q curve for the OUT station (cf. Fig. 4a). The scatter on  $Q_{GL}$ – $H_{GL}$  relationship might be partially attributable to the role of other runoff sources (or sinks) between the GL and OUT station. However, observation errors on the  $H_{GL}$  and  $Q_{OUT}$  values will also play a role. Overall, the relationship of Fig. 4b mainly indicates that our assumptions discussed above are generally justified. As such, this relationship allowed us to estimate the runoff discharge at the glacier outlet, based on the observed flow depth at the GL station. Contrary to Fig. 3, this relationship should be also valid on days with rain.

No glaciers contribute water to the Djankuat stream between the MID and OUT station (Fig. 1). Likewise, the difference in contributing area is small (Table 1). We therefore assumed that the runoff discharge at the MID station ( $Q_{MID}$ ) was equal to the observed discharge at the out station ( $Q_{OUT}$ ).

### 3.3 Sediment load calculations

We calculated the suspended sediment load per hydrological event at the OUT, MID, and GL gauging stations as:

**Fig. 3** Relationship between suspended sediment concentrations at the OUT ( $SSC_{OUT}$ ) and the GL ( $SSC_{GL}$ ) gauging stations for non-rainy days (see Fig. 1). The 1:1 line is indicated in yellow. Outliers are indicated in red with their corresponding timing. The linear regression is based on all other observations ( $n = 79$ )



$$SL = \frac{\sum_{k=1}^n Q_k \cdot SSC_k}{n \cdot 10^6} \cdot \Delta t, \quad (2)$$

where  $SL$  is the suspended sediment load (t event<sup>-1</sup>);  $Q_k$  is the measured or estimated water discharge at moment  $k$  (m<sup>3</sup> s<sup>-1</sup>);  $SSC_k$  is the corresponding measured suspended sediment concentration at moment  $k$  (g m<sup>-3</sup>);  $n$  is the number of pairwise ( $Q$  and  $SSC$ ) measurements taken during that event; and  $\Delta t$  is the duration (s) of the hydrological event.

Furthermore, we have assessed the relative importance of the main glacier in the total sediment load as:

$$SL_{GL,REL} = 100 \cdot \frac{SL_{GL}}{SL_{OUT}} \quad (3)$$

where  $SL_{GL,REL}$  (%) is the relative proportion of the event sediment load at the GL station ( $SL_{GL}$ ) as compared to the corresponding daily sediment load at the OUT station ( $SL_{OUT}$ ). Likewise, we calculated the relative contribution

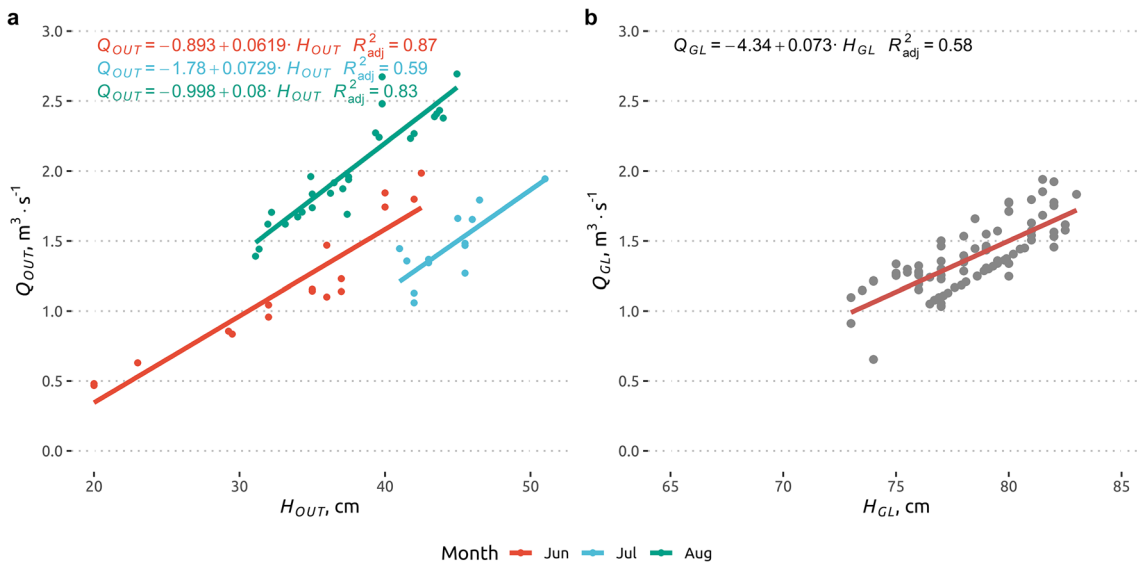


**Fig. 4** Runoff discharge ( $Q$ )–flow depth ( $H$ ) relationships: **a** for the OUT station during different months of the ablations season 2017; **b** for the GL station (cf. Fig. 1) during non-rainy days.  $H_{GL}$ ,  $H_{OUT}$ , and  $Q_{OUT}$  were manually observed at the station, while  $Q_{GL}$  was estimated based on Fig. 3 (see text)

( $SL_{MID,REL}$  (%)) of the sediment load at the MID station ( $SL_{MID}$ ) as:

$$SL_{MID,REL} = 100 \cdot \frac{SL_{MID} - SL_{GL}}{SL_{OUT}} \quad (4)$$

Overall, lower  $SL_{GL,REL}$  values indicate that a relatively large proportion of sediments do not originate from the glacier, but rather from the catchment hillslopes, the river bed or river banks. Values above 100% indicate that a proportion of the sediments originating from the glacier are deposited within the catchment before reaching the catchment outlet. Similarly, low  $SL_{MID,REL}$  values indicate that a significant amount of sediments originate from the river reach between the MID and OUT stations (and/or its bordering hillslopes; Fig. 1). Values above 100% indicate that sediment deposition occurs along this reach.

### 3.4 A SHI

As explained in the introduction, we aimed to systematically analyze observed event-hysteresis patterns and their potential link with sediment sources. For this, we develop a simple hysteresis index (*SHI*). This index was calculated for all sediment transport events recorded at the OUT station for which at least five  $SSC_{OUT}$  observations were available, including one observation at (or very close to) the peak discharge. For this, we first demarcated all hydrological events. This was done by smoothing the hourly water discharge values ( $Q_{OUT}$ ) using a linear moving median function with a window size of 3 h (as suggested by Rodda and Little (2015)). Next, we identified the start and end point of each event, using the local minimum method (Sloto and Crouse 1996).

The proposed *SHI* is illustrated in Fig. 5. First, we calculated a log-linear regression between  $Q$  and  $SSC$  for all observations made during that event (with a minimum of five). This regression line represents the  $SSC$  that could be expected for a given  $Q$  during that specific event, should there be no hysteresis at all. Next, we calculated the residues of all samples as the difference between the observed  $SSC$  and the estimated  $SSC$ , based on this event rating curve. The *SHI* then consists out of the difference between the mean residue of the samples in the rising limb and the mean residue of the samples in the falling limb, normalized for the maximum observed  $SSC$ :

$$SHI = \frac{\left( \frac{\sum_{i=1}^n dR_i + \dots + dR_n}{n} - \frac{\sum_{j=1}^m dF_j + \dots + dF_m}{m} \right)}{SSC_{max}} \quad (6)$$

with  $dR_i$ , the difference between observed and estimated  $SSC$  during the rising limb;  $dF_j$ , the difference between observed and estimated  $SSC$  during the falling limb;  $n$ ,  $m$ , the number of samples in respectively the rising and falling limb; and  $SSC_{max}$ , the maximum observed  $SSC$  of the event.

The *SHI* (Eq. 6) yields values between 1 and  $-1$ . As a result of its structure (cf. Fig. 5), values closer to 1 can be expected to correspond with events having a strong clockwise pattern, while values close to  $-1$  should correspond to more anti-clockwise events. Events with no strong hysteresis or a complex hysteresis pattern (e.g., figure-eight pattern) can be expected to have a *SHI*-value closer to zero. To test the validity of this interpretation, we visually inspected all events for which the *SHI* could be calculated and classified them according to their main hysteresis pattern, as proposed by Williams (1989): anticlockwise loops (AW), clockwise loops (CW), and figure-eight loops (F8). Events with no clear hysteresis pattern were classified as “not applicable” (NA).

## 4 Results

### 4.1 Field data

Between June 6, 2017, and September 22, 2017, 37 rainfall events were recorded with a mean rainfall depth of 13 mm (standard deviation 18.4 mm) and a mean duration of 5.96 h. The total precipitation depth of 482 mm was close to average precipitation amount for this area during the ablation period (Vasil’chuk et al. 2016). The mean rainfall intensity was  $2.63 \text{ mm h}^{-1}$  (standard deviation  $3.21 \text{ mm h}^{-1}$ ) with a maximum of  $17.7 \text{ mm h}^{-1}$ . The latter occurred during a 100-mm rainfall event in the night of 31 August–1 September. This event caused extreme erosion and triggered an outburst of the Bashkara Lake, located in a neighboring valley (Chernomorets et al. 2018). The event also damaged the gauging stations. For the OUT stations, the necessary reparations were conducted by noon on September 1 and measurements could continue. However, for the MID and GL station, measurements were stopped after August 30.

At the OUT station (cf. Fig. 1), the mean recorded water discharge during the observation period was  $1.39 \text{ m}^3 \text{ s}^{-1}$  (standard deviation  $0.46 \text{ m}^3 \text{ s}^{-1}$ ). The maximum recorded discharge was  $3.21 \text{ m}^3 \text{ s}^{-1}$ , observed on September 1 (Table 2; Fig. 6). However, due to the abovementioned damages, the real occurring maximum discharge might have been higher. The mean recorded  $SSC$  at OUT was  $725 \text{ g m}^{-3}$  (standard deviation  $2980 \text{ g m}^{-3}$ ; cf. Table 2; Fig. 6), with a maximum of  $53,800 \text{ g m}^{-3}$  (likewise measured in the night of September 1, 2017). Recorded  $SSCs$  at the MID and GL stations were relatively lower (respectively  $325$  and  $365 \text{ g m}^{-3}$ ). However, the median  $SSC$  did not differ significantly between the OUT, MID, and GL station (Table 2).

The mean event suspended sediment load at the OUT station was  $68.3 \text{ t event}^{-1}$  (standard deviation  $170 \text{ t event}^{-1}$ ). The total measured suspended sediment load ( $SL$ ) was  $9224 \text{ t}$  over the 110-day observation period (136 events). The total  $SL$  for the entire

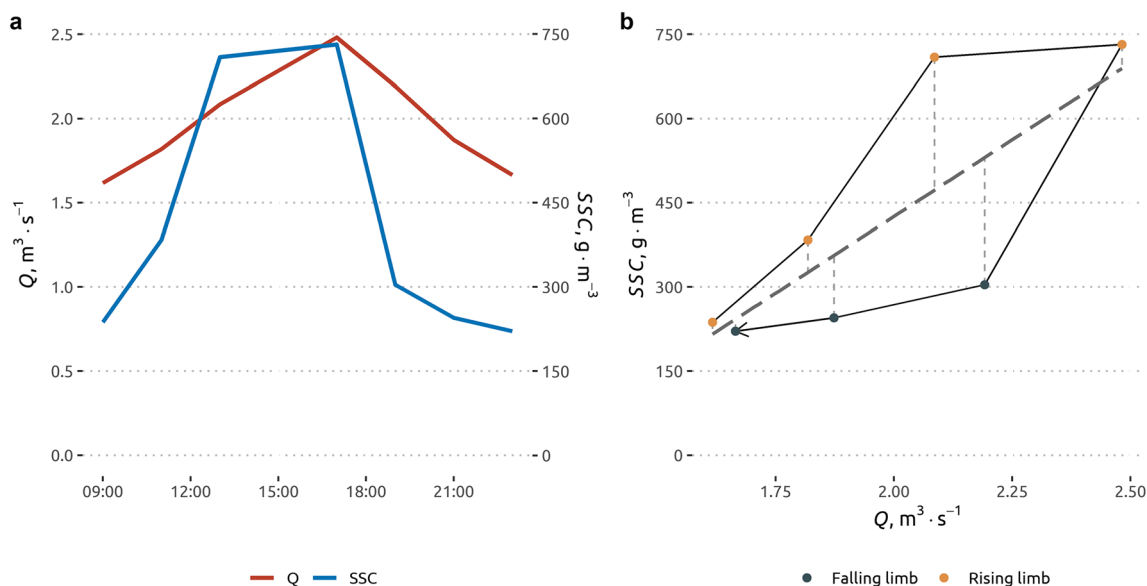


**Fig. 5** Example of an observed hysteresis loop, illustrating the calculation of the proposed simple hysteresis index (*SHI*; cf. Eq. 6). **a** Hydrograph and observed sediment concentrations of the event. **b** Corresponding hysteresis loop of the event. The dashed line shows the fitted runoff discharge ( $Q$ )–suspended sediment concentration ( $SSC$ )

rating curve for this event. In this case, the samples taken during the rising limb will have clearly positive residues, while those of the falling limb will be clear negative. As a result, the *SHI* for this event (Eq. 6) will have a clearly positive value, corresponding with the observed a clockwise hysteresis pattern

2017 ablation season is expected to be in the order of 9408 t, corresponding to a sediment yield of  $1033 \text{ t year}^{-1} \text{ km}^{-2}$ . The mean *SL* at GL and MID was 37 and  $37.4 \text{ t event}^{-1}$ , respectively (Table 3). The maximum *SL* at OUT station was measured during the hydrological event of 31 August (2017-08-31 22:00:00–2017-09-01 04:00:00). However, during these events, no measurements could be collected at the GL and MID station. As such, the average and maximum *SL* for these stations over the whole ablation period of 2017 were likely higher.

### 4.2 Patterns and trends of hysteresis in sediment concentrations

For 136 events recorded at the OUT station, enough samples were collected to calculate the *SHI*. Of these events 84 were visually classified as having a clockwise (CW) hysteresis loop pattern, 16 as anticlockwise (AW), seven as figure eight (F8) and 29 as having no clear hysteresis loop pattern (NA). As such, clockwise hysteresis patterns were the most observed

loop type, occurring during 61.8% of the events. Anticlockwise and figure-eight loops occurred for, respectively, 11.8% and 5.15% of the events (Table 4).

Overall, the mean *SSC* during anticlockwise events was higher (but not significantly, according to a Wilcoxon ranksum test at significance level 0.05) than those of clockwise events ( $668$  and  $548 \text{ g m}^{-3}$ , respectively; Table 4). Clockwise events also typically had a slightly (but significantly, according to a Wilcoxon rank sum test at significance level 0.05) lower mean water discharge ( $Q$ ) than anticlockwise events (Table 4). No significant differences in mean  $Q$  were detected between the other types of events.

We also computed the time lag for each event, i.e. the difference in timing between peak water discharge and peak *SSC*. For CW events, the *SSC* peaks on average 1.5 h before the  $Q$  peak (standard deviation 2.32 h). For AW events, the *SSC* peaks on average 2.06 h after the  $Q$  peak (standard deviation 1.95 h). We detected no significant differences in the duration of the events between the different hysteresis types (see Table 4).

**Table 2** Summary statistics of the water discharge ( $Q$ ,  $\text{m}^3 \text{ s}^{-1}$ ) and suspended sediment concentration ( $SSC$ ,  $\text{g m}^{-3}$ ) at different gauging stations at the Djankuat river for the 2017th ablation period (with “r” the gauging station; cf. Fig. 1)

Variable	Mean	Standard deviation	Median	Maximum	Time of maximum	Minimum	Time of minimum
$Q_{\text{OUT}}$ ( $\text{m}^3 \text{ s}^{-1}$ )	1.39	0.465	1.44	3.21	2017-09-01 14:00:00	0.345	2017-06-18 10:00:00
$Q_{\text{GL}}$ ( $\text{m}^3 \text{ s}^{-1}$ )	1.38	0.238	1.34	1.94	2017-08-09 19:35:00	0.655	2017-08-28 07:30:00
$SSC_{\text{OUT}}$ ( $\text{g m}^{-3}$ )	725	2980	237	53,800	2017-09-01 00:00:00	213	2017-06-23 09:00:00
$SSC_{\text{GL}}$ ( $\text{g m}^{-3}$ )	367	328	267	3010	2017-08-23 17:00:00	215	2017-07-12 13:30:00
$SSC_{\text{MID}}$ ( $\text{g m}^{-3}$ )	325	292	245	2600	2017-08-23 17:00:00	214	2017-07-07 20:00:00

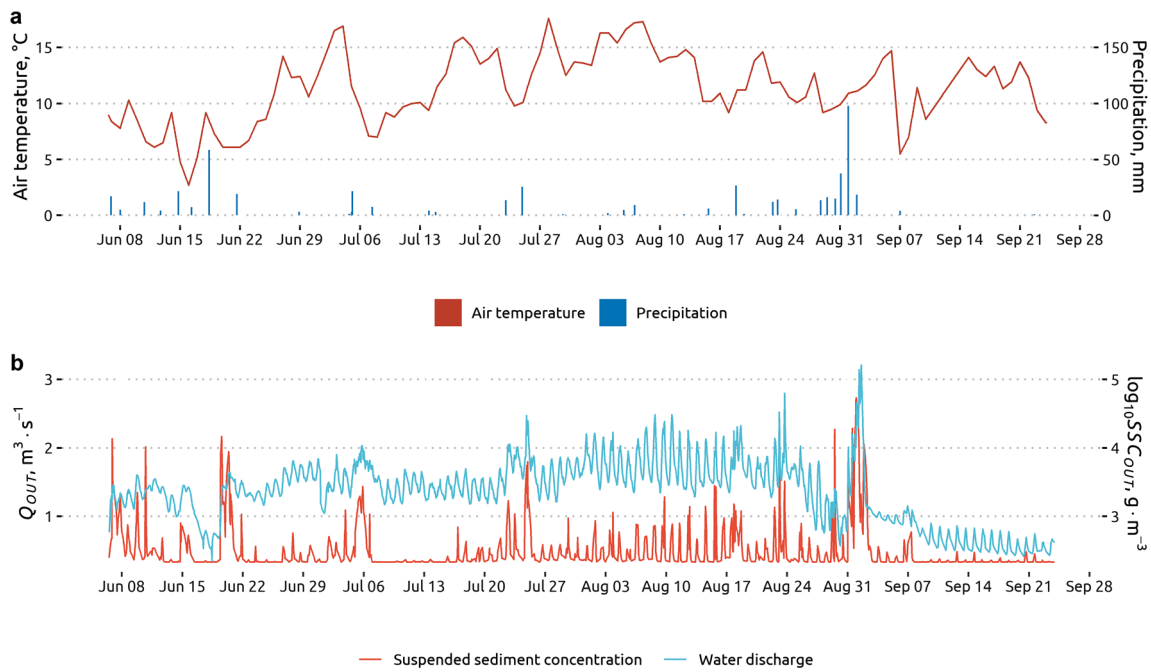


**Fig. 6** **a** Graphs of 2 m air temperature (°C), precipitation (mm) at the DGS. **b** Water discharge ( $\text{m}^3 \text{s}^{-1}$ ) and suspended sediment concentration ( $\text{g m}^{-3}$ ) at the Djankuat river outlet station (OUT) during the 2017 measuring period

In terms of sediment load, almost half of the total measured *SL* at the OUT station was exported during events with a clockwise hysteresis loop (4409 t or 47.8%). The total *SL* occurring during anticlockwise events was 1325 t (14.4% of the total *SL* during the observation period). More than 30% of the *SL* was exported during events for which no clear hysteresis pattern could be identified.

Figure 7 displays the calculated *SHI* versus the corresponding  $SL_{OUT}$  and maximum  $Q_{OUT}$  of each event. For clockwise events, higher peak runoff discharges and *SL* typically result in a higher *SHI*. As such, the degree of hysteresis overall increases with the magnitude of the event. For the other event types, patterns are less clear. For AW events, larger runoff peak discharges tend also to be associated with slightly lower *SHI* values and, hence, a more pronounced negative hysteresis pattern. However, this trend does not hold for *SL* (Fig. 7).

### 4.3 Hysteresis patterns and sediment budget analyses

For 58 out of the 136 events that were recorded at the OUT station, simultaneous recordings were also available for the MID and GL station (between June 30 and August 30). Comparison of the *SL* from GL and OUT indicated that sediment deposition occurred in 14 out of the 58 events (24%). The total difference corresponded with an estimated 305 t of material deposited in the section between GL and OUT (cf. Fig. 1). For 44 events (76%), the *SL* at OUT was higher than at GL, indicating that additional erosion in the catchment and the channel occurred. These differences amounted to a total of 642 t of eroded materials. Comparing the amount of deposition/erosion with the event hysteresis type revealed no clear pattern (Fig. 8).

To assess the overall importance of the Djankuat glacier in the sediment budget, we calculated  $SL_{GL,REL}$  (cf.

**Table 3** Suspended sediment load (*SL*) at the different gauging stations of the Djankuat catchment (cf. Fig. 1) for the 2017 ablation season

Gauging station	Number of events	<i>SL</i> during observation period <sup>1</sup> (t)	Total estimated <i>SL</i> for ablation period (t)	Mean ( $\text{t event}^{-1}$ )	Standard deviation ( $\text{t event}^{-1}$ )	Median ( $\text{t event}^{-1}$ )	Max ( $\text{t event}^{-1}$ )	Min ( $\text{t event}^{-1}$ )
GL	58	2148	–	37	37.9	26.5	210	6
MID	58	2168	–	37.4	32.6	30.5	220	7
OUT	135	9224	9408	68.3	170	30	1800	1.9

<sup>1</sup> Observation period: for GL and MID: 30/06/2017–30/08/2017; for OUT: 06/06/2017–24/09/2017

**Table 4** Main characteristics of the runoff and sediment transport events at the OUT station, for which at least five suspended sediment concentration (SSC) measurements were conducted. A distinction is made according to the type of observed hysteresis loop (AW,

anticlockwise loops; CW, clockwise loops; F8, figure-eight loops; NA, not applicable).  $Q$  water discharge,  $SHI$  simplified hysteresis index (cf. Eq. 6);  $SSC$  suspended sediment concentration,  $SL$  suspended sediment load

	AW	CW	F8	NA	Total
Number of events	16	84	7	29	136*
Proportion of events (%)	11.8	61.8	5.15	21.3	100*
Mean event duration (h)	19.3	20.3	22.3	12.2	18.5**
Mean $Q$ lag time (h)	-2.06	1.5	-2.29	-	-0.95**
Standard deviation in $Q$ lag time (h)	1.95	2.32	3.99	-	-
Mean $SHI$	-0.166	0.134	0.00663	-0.0291	-0.014**
Maximum $SHI$	-0.000628	0.464	0.186	0.516	0.516***
Minimum $SHI$	-0.597	0.000839	-0.117	-0.508	-0.597****
Mean $Q$ ( $m^3 s^{-1}$ )	1.65	1.32	1.66	1.47	1.52**
Maximum $Q$ ( $m^3 s^{-1}$ )	3.2	2.8	2.4	2.7	3.2***
Mean $SSC$ ( $g m^{-3}$ )	668	548	347	2650	1052**
Maximum $SSC$ ( $g m^{-3}$ )	11,000	19,000	1900	54,000	54000***
Mean $SL$ ( $t event^{-1}$ )	82.8	52.5	50.9	112	74.5**
Total $SL$ [t]	1320	4410	356	3130	9224*
Contribution to total $SL$ [%]	14.4	47.8	3.86	34	100*

\*Total sum  
 \*\*Total mean  
 \*\*\*Total maximum  
 \*\*\*\*Total min

Eq. 3) for 44 events. From this, we estimated that the glacier contributed on average 71.8% (median 77.6%) of the suspended sediment load recorded at the OUT station.

To obtain more insight in the sediment dynamics between the GL, MID and OUT station, we also compared the  $SL_{GL,REL}$

(Eq. 3) and  $SL_{MID,REL}$  (Eq. 4) with the corresponding  $SHI$  of the event (as recorded at the OUT station) and explored the observed relationships with respect to time period, rainfall conditions, magnitude of the event, etc. Figure 9 displays some key results. For non-rainfall events, the  $SHI$  is negative-

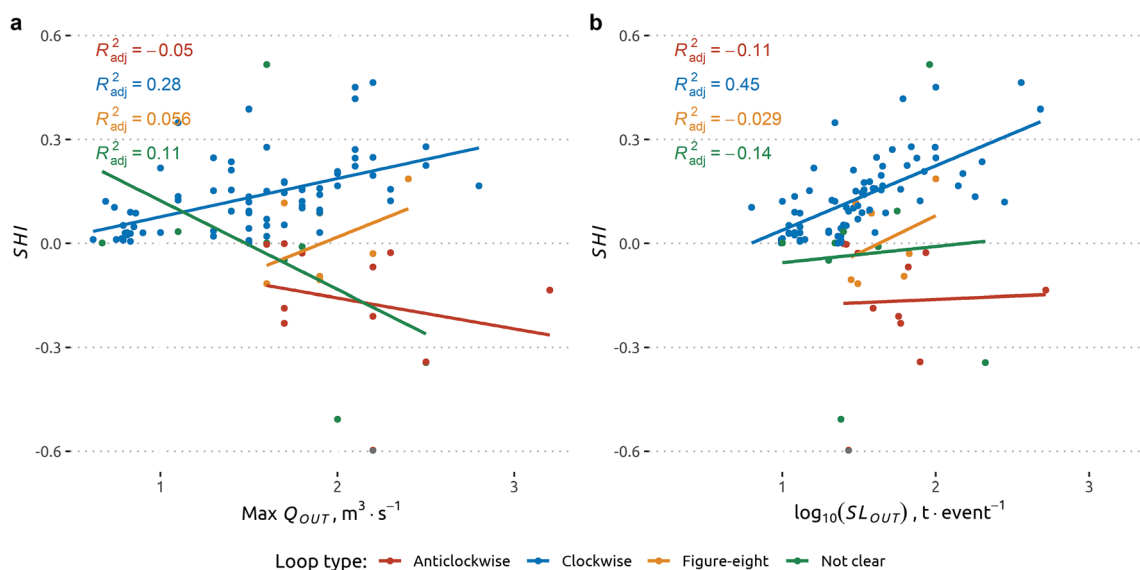


**Fig. 7** Simple hysteresis index ( $SHI$ ) for events recorded at the OUT station, versus maximum water discharge ( $max Q_{OUT}$  ( $m^3 s^{-1}$ ), plot a) and the logarithm of the suspended sediment load of the event ( $SL_{OUT}$  ( $t event^{-1}$ ), plot b)

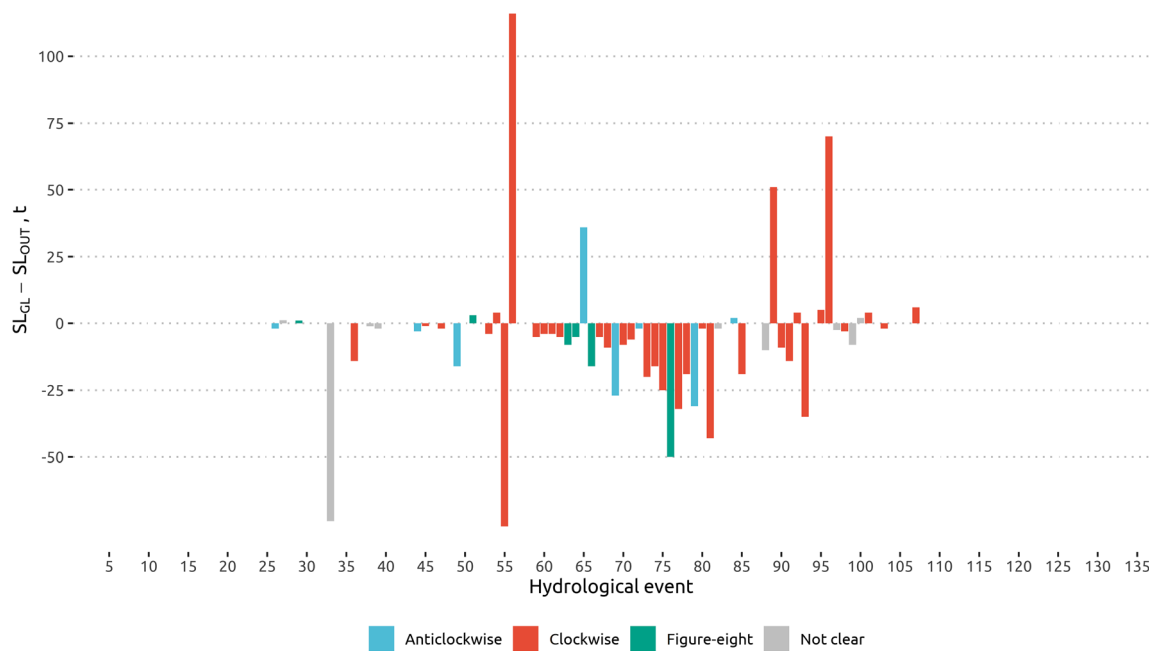


**Fig. 8** Difference in the sediment load at the GL and OUT station for different events for which samples were simultaneously collected at both stations. Negative values indicate additional erosion, while positive

values indicate sediment deposition. Hydrological events are colored according to their hysteresis type. Event numbers are chronological and refer to the events in Supplementary 1

sediment load ( $SL_{GL,REL}$ ; cf. Fig. 9a). As such, relatively larger contributions of the main glacier (Djankuat glacier) to the total sediment load are typically associated with less positive (clockwise) hysteresis loops.

Interestingly, during non-rainfall events, SHI shows no real correlation with the contribution of the middle reach (Fig. 9b). However, for significant rainfall events ( $> 8$  mm),  $SL_{MID,REL}$  shows a clear positive correlation with the SHI (Fig. 9d). During such rainfall events, additional erosion from the proglacial area can be expected, resulting in a higher  $SL_{MID,REL}$ . Hence, as indicates, larger contributions from the proglacial areas are also reflected in more positive (clockwise) hysteresis effects. By consequence, more positive hysteresis loops during rainfall events are also associated with lower contributions of the glacier (Fig. 9c).

## 5 Discussion

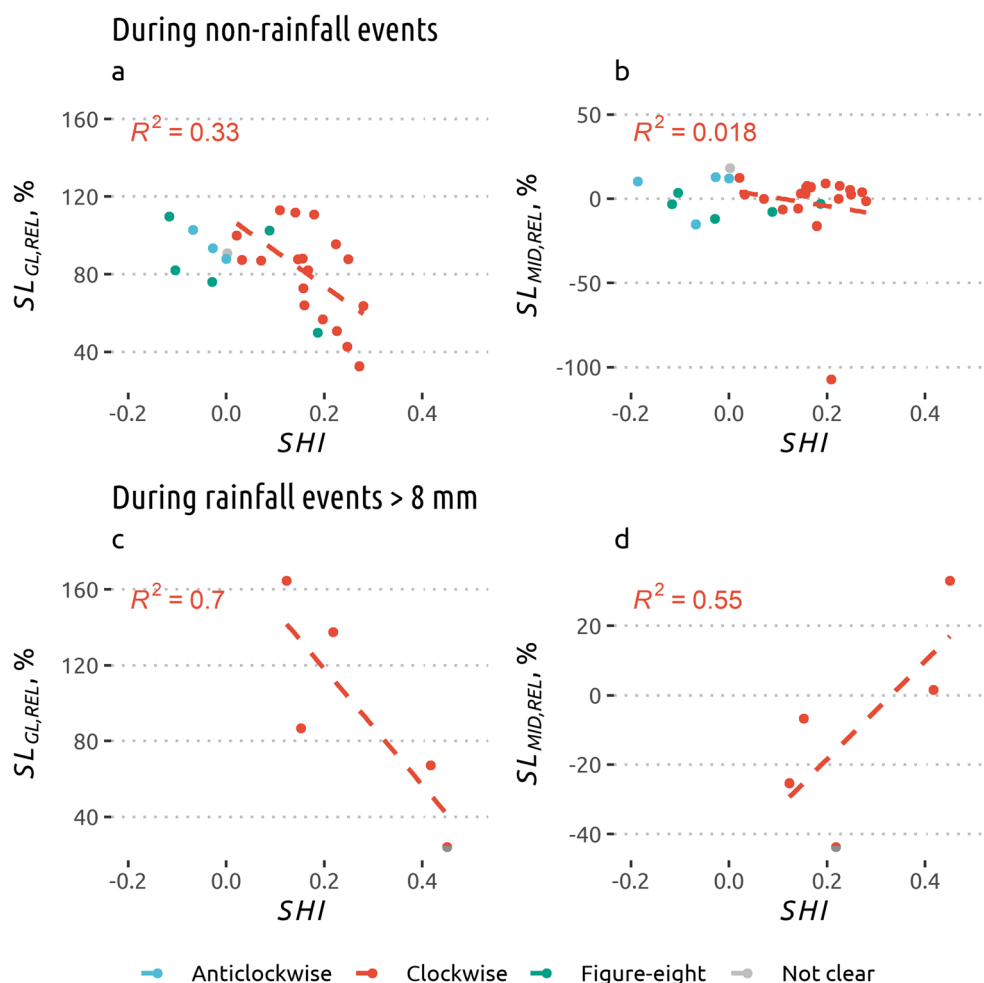
### 5.1 Sediment load and relative contribution of the glacier

The total measured suspended sediment yield for the Djankuat catchment for the ablation period of 2017 was  $1033 \text{ t year}^{-1} \text{ km}^{-2}$ . Given that the Djankuat stream has no significant water discharge outside the ablation period, this yield will also closely approximate the annual sediment yield. As always, this sediment yield should be interpreted with caution as it represents a value for only 1 year and sediment yields are generally characterized by a large inter-annual variability

(Vanmaercke et al. 2012). Likewise, measuring errors can induce significant uncertainties. A key factor influencing this uncertainty is generally the SSC sampling frequency (e.g., Phillips et al. 1999; Moatar et al. 2006). Overall, the sediment and runoff sampling frequency of this study can be considered quiet high as compared to other SY studies (Vanmaercke et al. 2011, 2014). Nevertheless, also in our case, measuring errors likely induced uncertainties. This is especially so for larger events, as the safety situation often limited the opportunities to collect samples and the very high recorded turbidities (above 16,000 NTU) might underestimate the actual SSC.

Despite these potential uncertainties, our measurements indicate that the sediment yield for the Djankuat catchment is rather high as compared to other estimates available for the region. Gabrielyan (1971) reported a mean annual suspended sediment yield for the Northern Caucasus of  $900 \text{ t year}^{-1} \text{ km}^{-2}$ . Mozzherin and Sharifullin (2015) estimated that the mean contemporary annual denudation rate of the Greater Caucasus ranges between  $0.1$  and  $0.25 \text{ mm year}^{-1}$ . According to their map, the mean annual suspended sediment yield in the study area would be around  $660 \text{ t year}^{-1} \text{ km}^{-2}$ . A more recent interpolation of gauging station data in the region concurs with this, resulting in an estimated mean annual suspended sediment yield for the study area of approximately  $700 \text{ t year}^{-1} \text{ km}^{-2}$  (Tsyplov et al. 2019). This relatively higher SY for the Djankuat catchment is most likely attributable to the presence of the glaciers and the large sediment availability in the sparsely vegetated proglacial area. As such, our estimated SY is relatively low as compared to other glaciated catchments. For example, Gurnell et al.

**Fig. 9** The relationship between  $SL_{GL,REL}$  (%) (cf. Eq. 3),  $SL_{MID,REL}$  (%) (cf. Eq. 4) and  $SHI$  (cf. Eq. 6) for non-rainfall events (a, b), as well as between  $SL_{GL,REL}$  (%),  $SL_{MID,REL}$  (%) and  $SHI$  for rainfall events (c, d)



(1996) report a  $SY$  of  $1800 \text{ t year}^{-1} \text{ km}^{-2}$  for the Glacier de Tsidjiore Nouve in the Alps (Switzerland). Hodgkins et al. (2003) report a  $SY$  of  $2250 \text{ t year}^{-1} \text{ km}^{-2}$  for an Arctic Glacier on Svalbard. Nevertheless, as compared to other reported denudation rates for glaciated catchments worldwide, the  $SY$  of the Djankuat falls within the expected order of magnitude for its catchment size and glacial extent (Hallet et al. 1996). Taking less than 0.02 % to the Terek river catchment area, the Djankuat river in 2017 contributed to 0.12 % of the Terek river sediment yield measured at the downstream Kartgalinsky gauging station in Dagestan.

Our measurements indicated that the Djankuat glacier is the dominant suspended sediment source, accounting for about 71.8% of the sediment export. By consequence, 28.2% of the sediment load likely originates from the proglacial zone (corresponding to about  $291 \text{ t km}^{-2} \text{ year}^{-1}$ ). Also, these values correspond well to those reported by other studies; e.g., O'Farell et al. (2009) report that in a small glaciated catchment in Alaska (catchment area  $16.7 \text{ km}^2$ ),  $10 \pm 7\%$  of the sediment yield comes from the proglacial zone. Likewise, in the Alpine catchment of the Arolla glacier (catchment area  $7.56 \text{ km}^2$ ), approximately 77% of the sediment load originates from the

stream at the glacial snout and the moraine deposition zone (Warburton 1990).

Nevertheless, these sediment contributions should be interpreted with caution as they may vary over time. For example, Mao and Carrillo (2017) showed for a Chilean Andean glacier that slope and channel processes are the dominant source at the beginning and end of the ablation season. Such potential temporal dynamic could not be observed in the Djankuat glacier, due to lack of data in June and September. Nevertheless, we detected no significant differences between the period of snowmelt (July) and the period where only the glacier delivered meltwater (August). Our measurements did indicate, however, that erosion due to rainfall becomes increasingly important through August–September.

Our analyses of hysteresis patterns might shed some additional light on the relative contribution of different sediment sources. Overall, the fact that clockwise hysteresis loops are the most frequently occurring type observed in the Djankuat catchment (cf. Table 4) concurs with other studies in similar environments. For example, a study in the catchment of the Gangotri Glacier (western Himalayan) showed that clockwise diurnal loops are the most commonly occurring during the entire ablation season

(Singh et al. 2005). Likewise, in Japan, Iida et al. (2012) report that intra-event clockwise loops are more common than anti-clockwise, which were only observed during the snow-melt period. On the other hand, a similar study for the Vantaa River in southern Finland (Kämäri et al. 2018) indicated that events in snowmelt periods are typically characterized by clockwise hysteresis loops, while counterclockwise loops are more common in other seasons.

A commonly accepted explanation for positive (clockwise) hysteresis loops is the depletion of sediment sources in the proglacial area (Klein 1984; Mao and Carrillo 2017). Also, in non-glacial environments, the occurrence of clockwise loops is often attributed to the depletion of sediments during runoff events that cause overland erosion (Williams 1989; López-Tarazón et al. 2009; Vanmaercke et al. 2010; Sun et al. 2016). Anti-clockwise loops are usually linked to the release of sediments after a certain threshold of water discharge has been exceeded. This can be due to streambank erosion or mass transport (Williams 1989; Iida et al. 2012). Other causes for anti-clockwise loops can be the rupture of an armor layer on the river bed (Morehead et al. 2003; Vanmaercke et al. 2010) or the entrainment of sediments that were previously deposited in floodplains (e.g., Oeurng et al. 2010).

Our statistical analyses, including the proposed *SHI*, allow to further test and explore these different hypotheses. For example, the idea of sediment depletion as a cause of clockwise loops seems consistent with the fact that larger clockwise events are characterized by a more positive *SHI* and thus a relatively larger proportion of sediments transported during the rising limb of the event (Fig. 7). As such, larger events seem to be capable to flush out and deplete available sediments relatively faster than smaller events. Furthermore, for most clockwise events, the sediment load at the outlet is larger than at the glacier snout (Fig. 8), pointing to the entrainment of additional sediments from the proglacial area. In addition, during none-rainfall events (when the dominant source of the river discharge is the glacier), relatively larger contributions of the glacier to the total sediment load are also associated with less positive *SHI* values (Fig. 9a). This suggests that the glacier itself provides a relatively constant supply of sediments (resulting in little to no hysteresis patterns). However, when also the proglacial areas supply sediments (resulting in a relatively lower  $SL_{GL,REL}$ ), events are characterized by more positive hysteresis patterns. The latter could be an indication of sediment depletion. This tendency becomes especially clear during rainfall events (when not only the proglacial channels but also hillslope erosion can contribute to the sediment load). Higher *SHI* values clearly appear more associated with relatively larger contributions from the proglacial area (Fig. 9c, d). Overall, this indicates that larger contributions from the proglacial area result in more clockwise hysteresis loops.

Although clearly less frequent, also anti-clockwise loops were observed in several cases (Table 4). Nonetheless, anti-clockwise

loops do seem to be associated with relatively large peak discharges (Table 4; Fig. 7). This indicates that they may be caused by the re-entrainment of sediments stored along the riverbanks. More specifically, the valley Sandur between the OUT and MID station (Fig. 1) may function as a temporal sediment storage that re-releases sediments during sufficiently large subsequent events. They may also be attributable to changes in sediment supply from the subglacial area or contributions of more distant sediment sources (e.g., Klein 1984; Mao and Carrillo 2017). However, the latter may be less likely, given the limited size of the catchment. Another explanation can be the supply of sediments due to streambank erosion or rock and boulder falls from lateral moraines during later stages of the event (Williams 1989; Vanmaercke et al. 2010; Iida et al. 2012).

Nevertheless, these sediment dynamics remain difficult to capture based on SSC observations and hysteresis patterns alone. For example, several events with a similar peak discharge resulted in a clockwise rather than an anti-clockwise loop (Fig. 7). For three of these events, our data indicates that sediment deposition occurred along the above-mentioned Sandur (Fig. 8). As such, not all clockwise loops are necessarily attributable to sediment depletion. Also, the overtopping of riverbanks and the consequent settling of suspended sediments in the flooded zone may cause a clockwise hysteresis loop. However, our analyses revealed no systematic pattern (e.g. in relation to timing, weather conditions, event magnitude or hysteresis loop characteristics) as to why some events seem to result in a net deposition or net entrainment of sediments (Fig. 8). Fully disentangling the sediment dynamics of the Djankuat and other similar catchments will therefore require the use of additional tools, such as sediment fingerprinting techniques.

Furthermore, the results and hysteresis patterns presented in this paper should be interpreted with caution as they represent only one ablation season. The expected glacier retreat may make new sediment sources available over time while older ones may become exhausted (Leggat et al. 2015). Furthermore, sediment contributions can vary strongly in relation to the timing and magnitude of precipitation or melt events. Continued high-resolution monitoring over consecutive years is therefore required to better understand the suspended sediment dynamics of proglacial catchments.

## 6 Conclusions

In this paper, we presented the results on runoff and sediment transport in glaciated Djankuat catchment (Northern Caucasus) for the ablation period of 2017, based on an extensive dataset of runoff discharge and sediment concentration observations collected at three gauging stations. The total suspended sediment export at the catchment outlet during the observation period (June 6–September 24) was 9224 t. An estimated 71.8% of this sediment load originated from

the glacier. However, during rainfall events, also hillslope erosion in the proglacial area can become a very significant sediment source.

We further explored intra-event sediment dynamics of > 130 events by statistically analyzing occurring hysteresis patterns. For this, we proposed a new simple hysteresis index (*SHI*; Eq. 6). This index weighs the relative importance of sediment concentrations during the rising and falling limb. It can be calculated based on a fairly limited number of samples (five or more) and can be used to robustly quantify hysteresis patterns in a continuous way. This not only avoids interpretation difficulties when manually classifying hysteresis loop patterns, but also allows more refined quantitative analyses.

Like earlier studies, we found that the majority (> 60%) of hysteresis loops are clockwise (Table 4). Analyses based on the *SHI* further showed that larger events (both in terms of sediment load and runoff peak discharge) are typically associated with more pronounced clockwise patterns (Figs. 7 and 8). This may point towards the importance of sediment depletion during events. Nonetheless, also sediment deposition during riverbank overtopping may result in a clockwise loop. As such, disentangling the exact causes of a certain hysteresis loop type remains very difficult. Nevertheless, our analyses (e.g., Fig. 9) clearly indicate that clockwise loop patterns are mainly caused by sediment contributions from the proglacial area rather than from the glacier itself. Additional tools (such as sediment fingerprinting) are required to further confirm and investigate this.

Overall, our results indicate that hysteresis loop types can indeed provide (to some extent) meaningful information on sediment sources within the catchment. They can help in better understanding the sediment dynamics of glaciated catchment. This is especially relevant in the context of climate change. Therefore, our methodology (and in particular the proposed *SHI*) may also be useful in other contexts.

**Acknowledgments** This study was conducted within the project of the Russian Scientific Foundation No. 19-17-00181 and a stay with an Erasmus+ International Credit Mobility scholarship. This study contributes to the State Task no. 0148- 2019-0005, Institute of Geography RAS. The help of Ekaterina Rets, Andrey Smirnov, Pavel Toropov, Varvara Bazilova, Anna Avilova, Ekaterina Komilova, and all other students who helped with the collection and processing of the field data is gratefully acknowledged.

**Author contributions** Conceptualization: Matthias Vanmaercke, Anatoly Tsyplenkov, Valentin Golosov; Methodology: Matthias Vanmaercke, Anatoly Tsyplenkov; Data collection and analyses: Anatoly Tsyplenkov with input from Matthias Vanmaercke; Writing: Anatoly Tsyplenkov, Matthias Vanmaercke, Valentin Golosov; Funding acquisition: Valentin Golosov, Sergey Chalov; Resources: Sergey Chalov; Supervision: Valentin Golosov, Matthias Vanmaercke.

**Funding** This study was funded by project of the Russian Scientific Foundation No. 19-17-00181.

**Data availability** Reproducible R code is available at the GitHub repository (<https://github.com/atsyplenkov/intra-event-djankuat>). Contact Anatoly Tsyplenkov ([atsyplenkov@gmail.com](mailto:atsyplenkov@gmail.com)) for more information.

## Compliance with ethical standards

**Conflict of interest** The authors declare that they have no conflict of interest.

**Ethical approval** This chapter does not contain any studies with human participants or animals performed by any of the authors.

**Informed consent** Informed consent was obtained from all individual participants included in the study.

## References

- Aich V, Zimmermann A, Elsenbeer H (2014) Quantification and interpretation of suspended-sediment discharge hysteresis patterns: how much data do we need? *Catena* 122:120–129. <https://doi.org/10.1016/j.catena.2014.06.020>
- Barry RG (2006) The status of research on glaciers and global glacier recession: a review. *Prog Phys Geogr* 30:285–306. <https://doi.org/10.1191/0309133306pp478ra>
- Beniston M (2003) Climatic change in mountain regions: a review of possible impacts. *Clim Chang* 59:5–31. <https://doi.org/10.1023/A:1024458411589>
- Bogen J (1989) Glacial sediment production and development of hydroelectric power in glacierized areas. *Ann Glaciol* 13:6–11
- Carrivick JL, Geilhausen M, Warburton J, Dickson NE, Carver SJ, Evans AJ, Brown LE (2013) Contemporary geomorphological activity throughout the proglacial area of an alpine catchment. *Geomorphology* 188:83–95. <https://doi.org/10.1016/j.geomorph.2012.03.029>
- Chernomorets SS, Petrakov DA, Aleynikov AA et al (2018) The outburst of Bashkara glacier lake (Central Caucasus, Russia) on September 1, 2017. *Kriosf Zemli XXII*:70–80. [https://doi.org/10.21782/KZ1560-7496-2018-2\(70-80\)](https://doi.org/10.21782/KZ1560-7496-2018-2(70-80)) (In Russian)
- Dedkov AP, Moszherin VI (1984) Erosion and sediment runoff on the Earth. *Izd-vo Kazansk. un-ta, Kazan* (In Russian)
- Dobryal P, Badola R, Tuboi C, Hussain SA (2017) A review of methods for monitoring streamflow for sustainable water resource management. *Appl Water Sci* 7:2617–2628. <https://doi.org/10.1007/s13201-016-0488-y>
- Durgerov MB, Freindlin VS, Chernova LP (1972) Suspended sediment load in the Djankuat glacier basin during the summer of 1970. *Mater Glaciol Issled* 19:253–254 (In Russian)
- Dyurgerov M (2003) Mountain and subpolar glaciers show an increase in sensitivity to climate warming and intensification of the water cycle. *J Hydrol* 282:164–176. [https://doi.org/10.1016/S0022-1694\(03\)00254-3](https://doi.org/10.1016/S0022-1694(03)00254-3)
- Farnsworth KL, Milliman JD (2003) Effects of climatic and anthropogenic change on small mountainous rivers: the Salinas River example. *Glob Planet Chang* 39:53–64. [https://doi.org/10.1016/S0921-8181\(03\)00017-1](https://doi.org/10.1016/S0921-8181(03)00017-1)
- Favaro EA, Lamoureux SF (2015) Downstream patterns of suspended sediment transport in a high Arctic river influenced by permafrost disturbance and recent climate change. *Geomorphology* 246:359–369. <https://doi.org/10.1016/j.geomorph.2015.06.038>
- Gabrielyan GK (1971) The intensity of denudation in the caucasus. *Geomorphol RAS* 1:22–27 (In Russian)

- Gao P, Josefson M (2012) Event-based suspended sediment dynamics in a central New York watershed. *Geomorphology* 139–140:425–437. <https://doi.org/10.1016/j.geomorph.2011.11.007>
- Geilhausen M, Morche D, Otto J-C, Schrott L (2013) Sediment discharge from the proglacial zone of a retreating Alpine glacier. *Zeitschrift für Geomorphol Suppl Issues* 57:29–53. <https://doi.org/10.1127/0372-8854/2012/S-00122>
- Glazirin GE, Semakova ER (2019) Estimation of Dispersed Glaciation Shrinkage Under Climate Change. *Geography, Environment, Sustainability* 12(1):5–12
- Gurnell A, Hannah D, Lawler D (1996) Suspended sediment yield from glacier basins. In: Walling DE, Webb BW (eds) *Erosion and sediment yield: global and regional perspectives*. IAHS Publ 236. IAHS Press, Wallingford, pp 97–104
- Hallet B, Hunter L, Bogen J (1996) Rates of erosion and sediment evacuation by glaciers: a review of field data and their implications. *Glob Planet Chang* 12:213–235. [https://doi.org/10.1016/0921-8181\(95\)00021-6](https://doi.org/10.1016/0921-8181(95)00021-6)
- Hamshaw SD, Dewoolkar MM, Schroth AW, Wemple BC, Rizzo DM (2018) A new machine-learning approach for classifying hysteresis in suspended-sediment discharge relationships using high-frequency monitoring data. *Water Resour Res* 54:4040–4058. <https://doi.org/10.1029/2017WR022238>
- Hinderer M (2012) From gullies to mountain belts: a review of sediment budgets at various scales. *Sediment Geol* 280:21–59. <https://doi.org/10.1016/j.sedgeo.2012.03.009>
- Hodgkins R, Cooper R, Wadham J, Tranter M (2003) Suspended sediment fluxes in a high-Arctic glacierised catchment: implications for fluvial sediment storage. *Sediment Geol* 162:105–117. [https://doi.org/10.1016/S0037-0738\(03\)00218-5](https://doi.org/10.1016/S0037-0738(03)00218-5)
- Iida T, Kajihara A, Okubo H, Okajima K (2012) Effect of seasonal snow cover on suspended sediment runoff in a mountainous catchment. *J Hydrol* 428–429:116–128. <https://doi.org/10.1016/j.jhydrol.2012.01.029>
- Jaoshvili S (2002) The rivers of the Black Sea. *EEA Tech Rep* 71:58
- Jones JAA (1999) Climate change and sustainable water resources: placing the threat of global warming in perspective. *Hydrol Sci J* 44: 541–557. <https://doi.org/10.1080/0266669909492251>
- Kämäri M, Tattari S, Lotsari E, Koskiahio J, Lloyd CEM (2018) High-frequency monitoring reveals seasonal and event-scale water quality variation in a temporally frozen river. *J Hydrol* 564:619–639. <https://doi.org/10.1016/j.jhydrol.2018.07.037>
- Khmeleva NV, Vinogradova NN, Samoilova AA, Shevchenko BF (2000) Mountain river basin and exogenous processes within it. *LMSU Faculty of Geography, Moscow* (In Russian)
- Khmeleva NV, Shevchenko BF (2006) The role of screes in the formation of the mountain rivers float and correlation of scree dynamics with solar cycles (according to stationary time series data). *Geomorphol RAS* 78:78–86. <https://doi.org/10.15356/0435-4281-2006-4-78-86> (In Russian)
- Klein M (1984) Anti clockwise hysteresis in suspended sediment concentration during individual storms: Holbeck catchment; Yorkshire, England. *Catena* 11:251–257. [https://doi.org/10.1016/0341-8162\(84\)90014-6](https://doi.org/10.1016/0341-8162(84)90014-6)
- Koppes MN, Montgomery DR (2009) The relative efficacy of fluvial and glacial erosion over modern to orogenic timescales. *Nat Geosci* 2: 644–647. <https://doi.org/10.1038/ngeo616>
- Kutuzov S, Lavrentiev I, Smirnov A, Nosenko G, Petrakov D (2019) Volume changes of Elbrus glaciers from 1997 to 2017. *Front Earth Sci* 7:153. <https://doi.org/10.3389/feart.2019.00153>
- Kutuzov S, Shahgedanova M (2009) Glacier retreat and climatic variability in the eastern Terskey–Alatoo, inner Tien Shan between the middle of the 19th century and beginning of the 21st century. *Glob Planet Chang* 69:59–70. <https://doi.org/10.1016/j.gloplacha.2009.07.001>
- Langlois JL, Johnson DW, Mehuys GR (2005) Suspended sediment dynamics associated with snowmelt runoff in a small mountain stream of Lake Tahoe (Nevada). *Hydrol Process* 19:3569–3580. <https://doi.org/10.1002/hyp.5844>
- Lavrentiev II, Kutuzov SS, Petrakov DA, Popov GA, Popovnin VV (2015) Ice thickness, volume and subglacial relief of Djankuat glacier (Central Caucasus). *Ice Snow* 128:7. <https://doi.org/10.15356/2076-6734-2014-4-7-19>
- Lawler DM, Petts GE, Foster IDL, Harper S (2006) Turbidity dynamics during spring storm events in an urban headwater river system: The Upper Tame, West Midlands, UK. *Sci Total Environ* 360:109–126. <https://doi.org/10.1016/j.scitotenv.2005.08.032>
- Leggat MS, Owens PN, Stott TA, Forrester BJ, Déry SJ, Menounos B (2015) Hydro-meteorological drivers and sources of suspended sediment flux in the pro-glacial zone of the retreating Castle Creek Glacier, Cariboo Mountains, British Columbia, Canada. *Earth Surf Process Landf* 40:1542–1559. <https://doi.org/10.1002/esp.3755>
- Lloyd CEM, Freer JE, Johnes PJ, Collins AL (2016) Using hysteresis analysis of high-resolution water quality monitoring data, including uncertainty, to infer controls on nutrient and sediment transfer in catchments. *Sci Total Environ* 543:388–404. <https://doi.org/10.1016/j.scitotenv.2015.11.028>
- López-Tarazón JA, Batalla RJ, Vericat D, Francke T (2009) Suspended sediment transport in a highly erodible catchment: The River Isábena (Southern Pyrenees). *Geomorphology* 109:210–221. <https://doi.org/10.1016/j.geomorph.2009.03.003>
- Mano V, Nemery J, Belleudy P, Poirel A (2009) Assessment of suspended sediment transport in four alpine watersheds (France): influence of the climatic regime. *Hydrol Process* 23:777–792. <https://doi.org/10.1002/hyp.7178>
- Mao L, Carrillo R (2017) Temporal dynamics of suspended sediment transport in a glacierized Andean basin. *Geomorphology* 287:116–125. <https://doi.org/10.1016/j.geomorph.2016.02.003>
- Moatar F, Person G, Meybeck M, Coynel A, Etcheber H, Crouzet P (2006) The influence of contrasting suspended particulate matter transport regimes on the bias and precision of flux estimates. *Sci Total Environ* 370:515–531. <https://doi.org/10.1016/j.scitotenv.2006.07.029>
- Moore RD, Fleming SW, Menounos B, Wheate R, Fountain A, Stahl K, Holm K, Jakob M (2009) Glacier change in western North America: influences on hydrology, geomorphic hazards and water quality. *Hydrol Process* 23:42–61. <https://doi.org/10.1002/hyp.7162>
- Morche D, Baewert H, Schuchardt A, Faust M, Weber M, Khan T (2019) Fluvial sediment transport in the proglacial Fagge river, Kaunertal, Austria. In: Heckmann T, Morche D (eds) *Geomorphology of proglacial systems*. Springer, Berlin, Germany, pp 219–229
- Morehead MD, Syvitski JP, Hutton EWH, Peckham SD (2003) Modeling the temporal variability in the flux of sediment from ungauged river basins. *Glob Planet Chang* 39:95–110. [https://doi.org/10.1016/S0921-8181\(03\)00019-5](https://doi.org/10.1016/S0921-8181(03)00019-5)
- Mozzherin VV, Sharifullin AG (2015) Estimation of current denudation rate of the mountains based on the suspended sediment runoff of the rivers (the Tien Shan, the Pamir-Alai, the Caucasus, and the Alps as an example). *Geomorphol RAS* 1:15–23. <https://doi.org/10.15356/0435-4281-2014-1-15-23> (In Russian)
- O’Farrell CR, Heimsath AM, Lawson DE et al (2009) Quantifying periglacial erosion: insights on a glacial sediment budget, Matanuska Glacier, Alaska. *Earth Surf Process Landf* 34:2008–2022. <https://doi.org/10.1002/esp.1885>
- Oeurng C, Sauvage S, Sánchez-Pérez J-M (2010) Dynamics of suspended sediment transport and yield in a large agricultural catchment, southwest France. *Earth Surf Process Landf* 35:1289–1301. <https://doi.org/10.1002/esp.1971>
- Otto J-C, Schrott L, Jaboyedoff M, Dikau R (2009) Quantifying sediment storage in a high alpine valley (Turtmanntal, Switzerland). *Earth Surf Process Landf* 34:1726–1742. <https://doi.org/10.1002/esp.1856>

- Phillips JM, Webb BW, Walling DE, Leeks GJL (1999) Estimating the suspended sediment loads of rivers in the LOIS study area using infrequent samples. *Hydrol Process* 13:1035–1050. [https://doi.org/10.1002/\(SICI\)1099-1085\(199905\)13:7<1035::AID-HYP788>3.0.CO;2-K](https://doi.org/10.1002/(SICI)1099-1085(199905)13:7<1035::AID-HYP788>3.0.CO;2-K)
- Polade SD, Pierce DW, Cayan DR, Gershunov A, Dettinger MD (2015) The key role of dry days in changing regional climate and precipitation regimes. *Sci Rep* 4:4364. <https://doi.org/10.1038/srep04364>
- Rets E, Chizhova JN, Loshakova N, Tokarev I, Kireeva MB, Budantseva NA, Vasil'chuk YK, Frolova N, Popovnin V, Toropov P, Terskaya E, Smirnov AM, Belozherov E, Karashova M (2017) Using isotope methods to study alpine headwater regions in the Northern Caucasus and Tien Shan. *Front Earth Sci* 11:531–543. <https://doi.org/10.1007/s11707-017-0668-6>
- Rets EP, Popovnin VV, Toropov PA, Smirnov AM, Tokarev IV, Chizhova JN, Budantseva NA, Vasil'chuk YK, Kireeva MB, Ekaykin AA, Veres AN, Aleynikov AA, Frolova NL, Tsyplenkov AS, Poliukhov AA, Chalov SR, Aleshina MA, Kornilova ED (2019) Djankuat glacier station in the North Caucasus, Russia: a database of glaciological, hydrological, and meteorological observations and stable isotope sampling results during 2007–2017. *Earth Syst Sci Data* 11:1463–1481. <https://doi.org/10.5194/essd-11-1463-2019>
- Rodda HJE, Little MA (2015) *Understanding mathematical and statistical techniques in hydrology*. Wiley, Chichester
- Rybak OO, Rybak EA (2018) Model-based calculations of surface mass balance of mountain glaciers for the purpose of water consumption planning: focus on Djankuat Glacier (Central Caucasus). *IOP Conf Ser Earth Environ Sci* 107:012041. <https://doi.org/10.1088/1755-1315/107/1/012041>
- Singh P, Haritashya UK, Ramasastri KS, Kumar N (2005) Diurnal variations in discharge and suspended sediment concentration, including runoff-delaying characteristics, of the Gangotri Glacier in the Garhwal Himalayas. *Hydrol Process* 19:1445–1457. <https://doi.org/10.1002/hyp.5583>
- Slaymaker O (2018) A global perspective on denudation data, primarily specific sediment yield in mountainous regions. *Landf Anal* 36:19–31. <https://doi.org/10.12657/landfana.036.003>
- Sloto RA, Crouse MY (1996) *Hysep: a computer program for streamflow hydrograph separation and analysis*. U. S. Geological Survey Water Resources Investigations Rep 96-4040, USGS, Washington, DC, USA
- Solomina ON (2000) Retreat of mountain glaciers of northern Eurasia since the Little ice age maximum. *Ann Glaciol* 31:26–30. <https://doi.org/10.3189/172756400781820499>
- Stokes CR, Popovnin V, Aleynikov A, Gurney SD, Shahgedanova M (2007) Recent glacier retreat in the Caucasus Mountains, Russia, and associated increase in supraglacial debris cover and supra-/proglacial lake development. *Ann Glaciol* 46:195–203. <https://doi.org/10.3189/172756407782871468>
- Stott TA, Mount NJ (2007) Alpine proglacial suspended sediment dynamics in warm and cool ablation seasons: implications for global warming. *J Hydrol* 332:259–270. <https://doi.org/10.1016/j.jhydrol.2006.07.001>
- Sun L, Yan M, Cai Q, Fang H (2016) Suspended sediment dynamics at different time scales in the Loushui River, south-Central China. *Catena* 136:152–161. <https://doi.org/10.1016/j.catena.2015.02.014>
- Syvitski JPM, Milliman JD (2007) Geology, geography, and humans battle for dominance over the delivery of fluvial sediment to the coastal ocean. *J Geol* 115:1–19
- Tielidze LG, Lomidze N, Asanidze L (2015) Glaciers retreat and climate change effect during the last one century in the Mestiachala river basin, Caucasus mountains, Georgia. *Earth Sci* 4:72–79. <https://doi.org/10.11648/j.earth.20150402.12>
- Tielidze LG, Wheate RD (2018) The greater Caucasus glacier inventory (Russia, Georgia and Azerbaijan). *Cryosph* 12:81–94. <https://doi.org/10.5194/tc-12-81-2018>
- Toropov PA, Shestakova AA, Smirnov AM (2017) Methodological aspects of heat balance components estimation on mountain glaciers. *Russ J Earth Sci* 17:1–9. <https://doi.org/10.2205/2017ES000605>
- Tsyplenkov A, Vanmaercke M, Golosov V (2019) Contemporary suspended sediment yield of Caucasus mountains. In: Chalov S, Golosov V, Collins A, Stone M (eds) *Lane use and climate change impacts on erosion and sediment transport*. IAHS Pub 381. IAHS Press, Wallingford, pp 87–93. <https://doi.org/10.5194/piahs-381-87-2019>
- Vanmaercke M, Poesen J, Broeckx J, Nyssen J (2014) Sediment yield in Africa. *Earth-Sci Rev* 136:350–368. <https://doi.org/10.1016/j.earscirev.2014.06.004>
- Vanmaercke M, Poesen J, Radoane M, Govers G, Ocakoglu F, Arabkhedri M (2012) How long should we measure? An exploration of factors controlling the inter-annual variation of catchment sediment yield. *J Soils Sediments* 12:603–619. <https://doi.org/10.1007/s11368-012-0475-3>
- Vanmaercke M, Poesen J, Verstraeten G, de Vente J, Ocakoglu F (2011) Sediment yield in Europe: spatial patterns and scale dependency. *Geomorphology* 130:142–161. <https://doi.org/10.1016/j.geomorph.2011.03.010>
- Vanmaercke M, Zenebe A, Poesen J, Nyssen J, Verstraeten G, Deckers J (2010) Sediment dynamics and the role of flash floods in sediment export from medium-sized catchments: a case study from the semi-arid tropical highlands in northern Ethiopia. *J Soils Sediments* 10: 611–627. <https://doi.org/10.1007/s11368-010-0203-9>
- Vasil'chuk YK, Rets EP, Chizhova JN et al (2016) Hydrograph separation of the Dzhankuat River, North Caucasus, with the use of isotope methods. *Water Resour* 43:847–861. <https://doi.org/10.1134/S0097807816060087>
- Vinogradova NN, Krylenko IV, Sourkov VV (2007) Some regularities of channel formation in the upper course of mountain rivers (Baksan river as an example). *Geomorphol RAS* 2:49–56. <https://doi.org/10.15356/0435-4281-2007-2-49-56> (In Russian)
- Walling DE (1995) Suspended sediment yields in a changing environment. In: Gurnell AM, Petts GE (eds) *Changing River Channels*. Wiley, Chichester, pp 149–176
- Warburton J (1990) An alpine proglacial fluvial sediment budget. *Geogr Ann Ser A Phys Geogr* 72:261–272. <https://doi.org/10.1080/04353676.1990.11880322>
- Williams GP (1989) Sediment concentration versus water discharge during single hydrologic events in rivers. *J Hydrol* 111:89–106. [https://doi.org/10.1016/0022-1694\(89\)90254-0](https://doi.org/10.1016/0022-1694(89)90254-0)

**Publisher's note** Springer Nature remains neutral with regard to jurisdictional claims in published maps and institutional affiliations.